Deep-Sea Research II 90 (2013) 68–76

Contents lists available at SciVerse ScienceDirect

Deep-Sea Research II

journal homepage: www.elsevier.com/locate/dsr2

Analysis of horizontal and vertical processes contributing to natural iron supply in the mixed layer in southern Drake Passage

Marina Frants [a,*], Sarah T. Gille [a], Mariko Hatta [b], William T. Hiscock [c], Mati Kahru [a], Christopher I. Measures [b], B. Greg Mitchell [a], Meng Zhou [d]

[a] Scripps Institution of Oceanography, University of California, San Diego, La Jolla, CA 92093-0230, United States
[b] University of Hawaii, Honolulu, HI 96822, United States
[c] University of Bern, CH-3012, Switzerland
[d] University of Massachusetts Boston, MA 02125, United States

ARTICLE INFO

Available online 16 June 2012

Keywords:
Southern ocean
Drake passage
Iron
Mixing
Diapycnal mixing
Ona basin

ABSTRACT

Horizontal advection, vertical mixing, and mixed-layer entrainment all affect iron concentrations and biological productivity in the Ona Basin, near the Shackleton Transverse Ridge (STR) in southern Drake Passage. Trace metal sampling in the region indicates that dissolved iron concentrations are significantly higher on the continental shelf near the Antarctic Peninsula and the South Shetland Islands than they are in the deep waters away from the shelf. Comparisons between satellite-derived sea surface height (SSH) and Chlorophyll-a (Chl-a) levels in the Ona Basin show $>95\%$ correlation between Chl-a concentrations and horizontal advection of these iron-rich shelf waters during the months of November and December for the years 1997–2010. However, no significant correlations are found for January–April, while high Chl-a concentrations in the Ona Basin persist through March. Enhanced vertical (diapycnal) mixing and mixed-layer entrainment are considered as alternative mechanisms for delivering iron into the Ona Basin mixed layer and sustaining the high Chl-a concentrations. Estimates of iron flux based on *in situ* measurements of dissolved iron concentrations suggest that diapycnal mixing alone can supply iron to the base of the mixed layer at a rate of 64 ± 2 nmol m^{-2} day^{-1} during the summer. In addition, the summer mixed layer in the Ona Basin deepens from January to April, allowing for iron-rich water to be steadily entrained from below. Estimates based on monthly mixed-layer climatologies produce average daily entrainment rates ranging from 5 to 25 nmol m^{-2} day^{-1}. While neither diapycnal mixing nor entrainment alone is always sufficient to meet the estimated iron demand for the Ona Basin bloom, numerical simulation suggests that the combined effect of the two processes can consistently supply sufficient iron to sustain the bloom.

1. Introduction

The waters of the Shackleton Fracture Zone (SFZ) in southern Drake Passage (Fig. 1A) display an uneven distribution of surface Chlorophyll-a (Chl-a) in the vicinity of the Shackleton Transverse Ridge (STR). Satellite imagery of the region (Kahru et al., 2007) shows elevated Chl-a levels in the shallow waters on the continental shelf, where iron can be entrained from the sediments (Hopkinson et al., 2007). In deeper waters north of the shelf, a sharp Chl-a gradient occurs, with low Chl-a levels found to the west of the Shackleton Transverse Ridge (STR) and higher Chl-a levels to the east, beginning in the Ona Basin and continuing downstream into the southern Scotia Sea (Holm-Hansen et al., 2004a; Kahru et al., 2007).

Biological productivity in the Southern Ocean has been shown to be iron-limited (Boyd, 2002; Chisholm and Morel, 1991; de Baar et al., 1995; Helbling et al., 1991; Martin et al., 1990), with persistent blooms observed in naturally iron-enriched areas such as Crozet Island (Planquette et al., 2007; Venables et al., 2007) and the Kerguelen Plateau (Blain et al., 2008). Shipboard iron incubations indicate that phytoplankton growth rates in the Ona Basin are also iron-limited away from the continental shelf (Helbling et al., 1991; Hopkinson et al., 2007). Observations in high-Chl-a regions suggest that iron is supplied to waters away from the shelf via horizontal advection and eddy-driven processes such us eddy pumping, cross-frontal mixing, and the formation of small-scale filaments formed by eddy interactions (Abraham et al., 2000; Frants et al., 2013; Kahru et al., 2007; Lapeyre and Klein, 2006; Maraldi et al., 2009; Venables

* Corresponding author.
E-mail address: mfrants@ucsd.edu (M. Frants).

0967-0645/$ - see front matter © 2012 Elsevier Ltd. All rights reserved.
http://dx.doi.org/10.1016/j.dsr2.2012.06.001

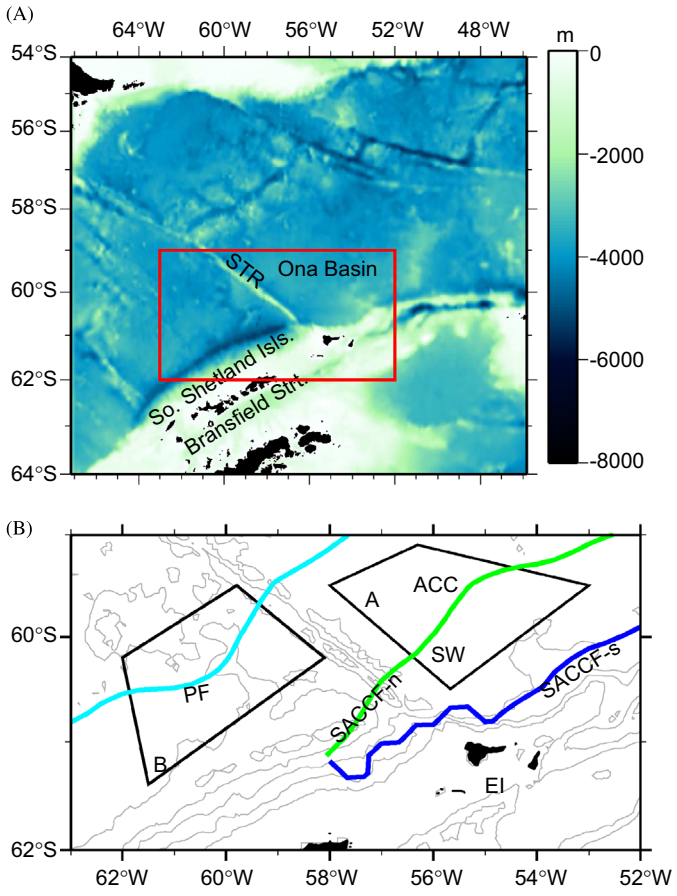

Fig. 1. Map of Drake Passage (A) illustrating the location of the Ona Basin, the Shackleton Transverse Ridge (STR), the South Shetland Islands, and the Bransfield Strait. The region used for the horizontal advection analysis described in Section 3.1 is outlined in red. A close-up of the analysis region (B) shows the location of Elephant Island (EI) and the time-mean locations of the Polar Front (PF, light blue line), the northern branch of the SACCF (SACCF-n, green line) and the southern branch of the SACCF (SACCF-s, dark blue line). ACC indicates the section of the Ona Basin where the waters of the Antarctic Circumpolar Current dominated the upper ocean circulation, as described by Frants et al. (2013). SW indicates the section where shelf waters dominate. Quadrangle A represents the downstream region used in the analysis discussed in Sections 2.1 and 2.2. Quadrangle B represents the upstream region.

et al., 2007). In a study of 10 years' worth of satellite data from the region near the Ona Basin, Kahru et al. (2007) found consistently high correlations between cyclonic eddy activity and Chl-a anomalies in the Weddell-Scotia Confluence during September and October. Their findings suggest that eddy-driven upwelling and cross-frontal northward iron transport could account for a significant part of the variability of the spring bloom. However, the higher Chl-a levels in the region persist throughout the summer, and Kahru et al. (2007) found no clear correlation between eddy activity and bloom intensity from January to March. In this study, we consider the vertical iron fluxes driven by diapycnal mixing and mixed-layer entrainment, and examine the hypothesis that these fluxes can provide the additional iron needed to sustain the late summer bloom in our study region.

Hydrographic studies in the vicinity of the STR and the South Shetland Islands have found evidence that iron is entrained from the sediments in the shallow waters on the continental shelf and distributed off-shore by horizontal advection (Hopkinson et al., 2007; Zhou et al., 2010a; Measures et al., 2013). In this study, we use a 13-year time series of satellite data to examine the relationship between Chl-a levels in the Ona Basin and off-shore advection driven by frontal movement. We then consider *in situ* temperature, salinity and dissolved iron data from our study region in combination with mixed-layer climatologies to estimate the effects of small-scale diapycnal mixing and mixed-layer entrainment, which may provide a vertical supply of additional iron into the mixed layer to sustain the Chl-a concentrations in months when horizontal advection alone is not sufficient. Finally, we use a one-dimensional numerical model to examine the combined effects of mixing and entrainment on the iron supply in the top 30 m in the Ona Basin during the months of January–April.

2. Data and methods

2.1. Upper Ocean circulation

To evaluate the upper ocean circulation in our study region, we obtained weekly maps of gridded sea level anomalies (SLA) for the months of November–April from 1997 to 2010 from AVISO (Archiving, Validation and Interpretation of Satellite Oceanographic Data) (Ducet et al., 2000). AVISO provides SLA maps gridded on a $1/3^\circ \times 1/3^\circ$ Mercator grid, computed from merged satellite data. Monthly average SLAs were computed from the weekly data sets. To obtain absolute sea surface height (SSH), a mean dynamic height field computed relative to 1500 db from the World Ocean Circulation Experiment (WOCE) hydrographic climatology (Gouretski and Koltermann, 2004) was added to the anomalies.

The Antarctic Circumpolar Current (ACC) is commonly characterized as consisting of three primary fronts: the Subantarctic Front (SAF), the Polar Front (PF) and the Southern ACC Front (SACCF) (Orsi et al., 1995). However, high-resolution satellite data (e.g. Hughes and Ash, 2001) have shown a more complicated structure consisting of multiple jets and filaments. A hydrographic study by Sokolov and Rintoul (2007) described each of the three main fronts as having multiple distinct branches, and a follow-up study (Sokolov and Rintoul, 2009) identified each frontal branch with a specific SSH contour. Our choice of the WOCE climatology to calculate SSH values allowed us to follow the Sokolov and Rintoul (2009) definitions to identify front locations. The southern branch of the PF and both branches of the SACCF run across our study region as shown in Fig. 1. West of the STR, the SACCF closely follows the 2000 m bathymetry contour until it reaches 58°W, where it splits into two branches. The northern branch (SACCF-n) moves northward, away from the shelf and into the Ona Basin, as shown in Fig. 1B. The waters north of the SACCF-n are dominated by the iron-depleted waters of the ACC, while iron-replete shelf waters are predominant south of the front (Frants et al., 2013).

2.2. Chlorophyll-a

Composite images of monthly surface Chl-a data from 1997 to 2010 were created by merging full-resolution standard level-2 Chl-a data from SeaWiFS, MODIS-Aqua and MODIS-Terra downloaded from the NASA Ocean Color Web (M. Kahru 2012, personal communication). Chl-a was computed using standard OC4/OC3 type algorithms (O'Reilly et al., 1998) of the 2007 reprocessing. Satellite estimates of surface Chl-a using standard algorithms show good agreement with shipboard Chl-a measurements in the region (Holm-Hansen et al., 2005), and correlate well with integrated Chl-a in the top 100 m of the water column (Holm-Hansen et al., 2004b). The Chl-a values were regridded from a 1-km grid to match the SLA grid, using a median filter with a radius of 18.5 km.

For our 13-year time series of SSH and Chl-a data, we estimated the proportion of shelf waters relative to ASW and WW in the analysis region from satellite altimetry. For each month, we determined the fraction of all grid points in the analysis region for which SSH was less than 64 cm. SSH values in the study area increase from south to north, with the 64 ± 2-cm contour identifying the location of the SACCF-n according to the criteria defined by Sokolov and Rintoul (2009). Therefore, choosing the SSH points below the 64-cm contour allowed us to account for both the waters being advected equatorwards behind the SACCF-n and the potential northward transport of shelf waters as a consequence of cold-core eddies being generated by the front.

2.3. Dissolved iron

CTD data were collected in February and March 2004 by the R/V Laurence M. Gould and in July and August 2006 by the R/V Nathaniel B. Palmer at locations shown in Fig. 2A, with water samples for trace metal analysis collected at selected stations. Frants et al. (2013) have provided a detailed description of the sampling and methods. Seawater samples for dissolved iron were collected using General Oceanic 12L Teflon coated GO-FLO bottles mounted on a 12-position trace metal clean rosette provided by the University of Hawaii. Sub-sampling was completed under trace element clean conditions; the GO-FLO bottles were pressurized to 70 kPa (10 psi) using 0.2 m filtered compressed air and seawater sub-samples were filtered under pressure through 0.45 m acid leached 47 mm polycarbonate track etched filters (GE Poretics; K04CP04700) held in a polypropylene filter holder (MFS). The filtrate was collected in acid leached 125 ml low-density polyethylene (LDPE) bottles. A detailed description of the TM rosette sampling system and trace metal clean sub-sampling protocols are provided elsewhere (Measures et al., 2008, 2013).

Dissolved trace element determinations for iron were performed on samples returned to the University of Hawaii using a pre-concentration method coupled with high resolution inductively coupled mass spectrometry (ICP-MS). The sample collection method and protocols using the TM rosette sampling system and the analytical techniques for measuring dissolved Al and Fe have been shown to be comparable with results obtained by other currently accepted sampling methodologies and analytical techniques investigated during the NSF-sponsored Sampling and Analysis of Iron (SAFe) intercomparison cruise (Johnson et al., 2007), with a measurement uncertainty of 0.08 nmol l^{-1}.

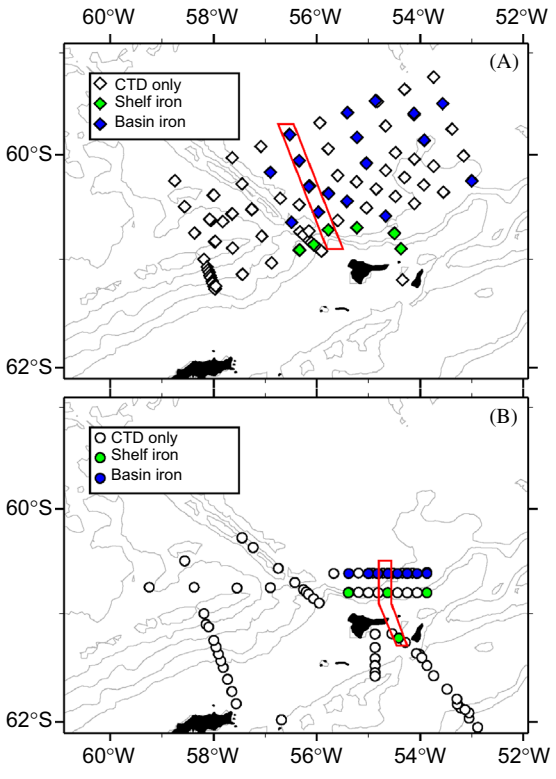

Fig. 2. Locations of CTD stations and iron stations sampled during the summer 2004 cruise (A) and the winter 2006 cruise (B). Blue symbols indicate Ona Basin stations, and green symbols indicate the stations on the continental shelf. Transects plotted in Fig. 6 are outlined in red. Only the iron stations sampled east of the Shackleton Transverse Ridge are shown.

2.4. Atmosphere and wind data

Estimates of precipitation rates, wind velocities, and surface heat fluxes are available from the National Centers for Environmental Prediction/National Center for Atmospheric Research (NCEP/NCAR) reanalysis project (Kalnay et al., 1996). The data are gridded by NCEP/NCAR as described by Kalnay et al. (1996) and are available four times daily. Additional wind velocity data were obtained from the European Centre for Medium-Range Weather Forecasts (ECMWF). Wind stress $\boldsymbol{\tau}$ was computed as $\boldsymbol{\tau} = \rho_a C|\mathbf{u}|\mathbf{u}$, where $\mathbf{u}$ is the wind velocity at 10 m above the sea surface, $\rho_a = 1.2$ kg/m^3 is the density of air, and C is the drag coefficient. The values for C were taken from Yelland and Taylor (1996) for $|\mathbf{u}| \geq 6$ m/s and from Yelland et al. (1998) for $|\mathbf{u}| < 6$ m/s.

3. Results and discussion

3.1. Assessing the effects of horizontal advection from satellite altimetry

Our analysis of the satellite data has focused on the deep offshore region in the Ona Basin shown as quadrangle A in Fig. 1B. The surface waters in this region are a mixture of Antarctic Surface Water (ASW) and Winter Water (WW) associated with the ACC, and denser shelf waters propagating off-shore from the Antarctic Peninsula and the South Shetland Islands (Barré et al., 2008; Zhou et al., 2010b). The shelf waters (SW) are iron-replete with mixed-layer dissolved iron concentrations on the order of 1 nmol l^{-1}, while the ACC waters to the north of the front are iron-limited, with mixed-layer concentrations on the order of 0.1 nmol l^{-1} (Hopkinson et al., 2007; Measures et al., 2013). The position of the SACCF-n relative to the water distribution in the study region indicates that this front serves as a barrier between the ASW and WW of the ACC, and the shelf waters, with ASW and WW dominating the water composition to the north of the front, and SW dominating to the south (Frants et al., 2013). SW can be advected off the shelf and into the Ona Basin by both geostrophic and wind-driven processes. In this section, we examine each process separately to evaluate their correlation with the Chl-a levels in the basin.

Kahru and Mitchell's (2006) analysis of climatological monthly mean surface Chl-a levels from 1997 to 2006 showed consistently higher levels of biological production in the Ona Basin compared to the waters west of the STR. Our analysis, illustrated in Fig. 3 and covering the years from 1997 to 2010, is consistent with their results. For all months, the Chl-a concentrations are higher in the downstream region, where the SACCF-n has moved equatorwards. Downstream Chl-a levels become slightly higher from January to February before decreasing again, and the concentrations for February and March are comparable to the concentration in

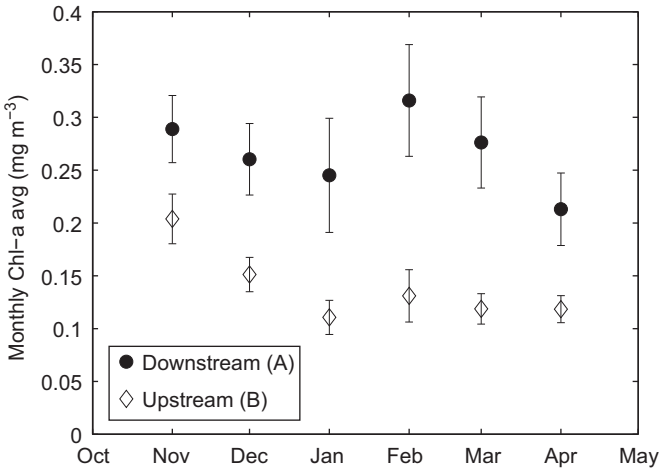

Fig. 3. Monthly climatological mean surface Chl-a concentrations downstream (quadrangle A in Fig. 1B) and upstream (quadrangle B in Fig. 1B) of the Shackleton Transverse Ridge during the years 1997–2010. The error bars represent the standard error of the mean.

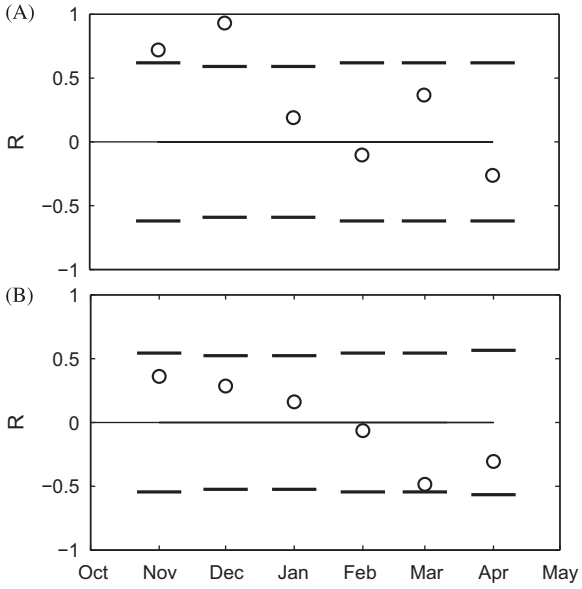

Fig. 4. Monthly correlation coefficients (circles) of the mean Chl-a levels in the Ona Basin during the years 1997–2010 with (A) the fraction of shelf water in the basin as estimated from the location of the northern branch of the SACCF and (B) the mean zonal wind stress. Horizontal black lines represent the 95% confidence interval.

November. Upstream Chl-a concentrations decrease from November to January and remain low for the duration of the austral summer. After the spring bloom, in the months of January, February and March, the downstream Chl-a values rise to more than twice the upstream levels. The differences in the Chl-a concentrations between the two regions suggest the presence of physical or biochemical mechanisms that increase the duration and intensity of the bloom in the Ona Basin.

Because the proportion of iron-rich shelf water in the Ona Basin changes over time as the front position shifts, we hypothesize that bloom intensity is driven primarily by geostrophic advection of iron off the shelf and that Chl-a concentrations should show highest concentrations occurring when the SACCF-n is furthest north. To examine this effect, we computed the correlation coefficients between the mean monthly Chl-a concentrations and the fraction of shelf waters present in the region, as determined by the method described in Section 2.2. For comparison, we also consider Chl-a concentrations in the low-iron, low Chl-a region to the west of the STR (quadrangle B in Fig. 1B). This region is located entirely north of the SACCF-n and is dominated by the waters of the ASW and WW, with little or no shelf waters present (Frants et al., 2013).

Fig. 4A shows the monthly correlation coefficients between monthly averaged Chl-a concentration and the monthly averaged proportion of shelf waters present in the downstream region from 1997 to 2010. The coefficients are highest in November and December, exceeding the 95% confidence level, then sharply decrease in January and remain low through the rest of the summer. The correlation pattern was independent of the choice of the SSH contour selected to define the SACCF-n within the 2-cm error margin estimated by Sokolov and Rintoul (2009). This decrease in correlation, combined with the persistently high Chl-a concentrations from January to March, is consistent with a scenario in which horizontal off-shore advection is a major factor in determining the strength of the Ona Basin bloom in the spring, but is not sufficient to maintain the bloom through the end of the summer.

Correlations based on SSH account only for the geostrophic transport in the region but not the northward Ekman transport driven by zonal eastward winds near the shelf, which can advect additional iron northward into the Ona Basin. To evaluate the effects of Ekman transport into the Ona Basin, we computed the monthly correlation coefficients between mean Chl-a concentrations and mean zonal wind stress for the downstream quadrangle A in Fig. 1B. The wind stress estimates were computed from spatially averaged NCEP/NCAR velocities as described in Section 2. All of the resulting coefficients (Fig. 4B) are below the 95% confidence level, suggesting that wind-driven horizontal advection is not a significant factor in initiating or sustaining the Ona Basin bloom. Performing the same calculation using ECMWF wind data also did not produce any correlation coefficients above the 95% confidence level.

3.2. *Effects of vertical processes on iron distribution*

The results of Section 3.1 indicate that additional mechanisms are needed to explain the persistence of the bloom from January through the end of March, when horizontal advection alone is not sufficient to maintain the Chl-a concentrations. These mechanisms can include iron fluxes driven by both physical and biological processes. Recent satellite observations and model results indicate that dust events in the Patagonian desert can transport iron-rich dust to sub-Antarctic waters (Gasso and Stein, 2007); however, Measures et al. (2013) suggest that eolian deposition to the sampling region is minimal. Laboratory studies have found that remineralization of particulate iron and recycling by microzooplankton grazing can play a significant role in supplying bioavailable iron to phytoplankton (Barbeau et al., 2001; Dalbec and Twining, 2009), and *in situ* studies during iron enrichment experiments in the Southern Ocean have shown that these processes can account for over 30% of the iron supply in the euphotic zone (Bowie et al., 2001; Strzepek et al., 2005). If remineralization or dust deposition were sufficient to sustain high Chl-a levels through the summer, then other iron-rich areas of the Southern Ocean might be expected to experience prolonged blooms similar to the Ona Basin. However, observations on the Crozet Plateau (Venables et al., 2007), the Kerguelen Plateau (Mongin et al., 2008), and the south side of South Georgia Island (Whitehouse et al., 2008) do not show the blooms in these regions persisting past January. The extended duration of the Ona Basin bloom suggests that this region has unique conditions that can sustain high Chl-a level through February and March. While it is possible that the Ona Basin is subject to unique biogeochemical processes or that it receives occasional inputs of bioavailable iron

from dust storms, here we explore the possibility that physical oceanographic processes alone are able to sustain the bloom by vertically delivering iron into the mixed layer. In particular, we consider how the dissolved iron concentrations in the mixed layer can be affected by diapycnal mixing and by entrainment due to changing mixed-layer depths.

To estimate the dissolved iron demand for the Ona Basin bloom, we followed the method outlined by Dulaiova et al. (2009), who also determined the residence time (*RT*) for iron in the region to be 4 days based on the apparent ages of water samples taken on and off the shelf. The daily dissolved iron demand (*DFe*) can be calculated as

$$DFe = [Chla_{conc}] \times h \times [\mathrm{C:Chla}] \times [molC : gC] \times [\mathrm{Fe:C}]/RT, \quad (1)$$

where h is the mixed-layer depth, $Chla_{conc}$ is the Chl-a concentration, and $molC : gC = 1/12$ is the ratio of moles to grams of carbon.

The value of *DFe* changes throughout the year, as the cellular iron:carbon (Fe:C) ratio decreases with reduced light availability and decreasing water temperatures, increasing iron demand and reducing growth rates (Sunda and Huntsman, 2011). In addition, Fe:C ratios will vary among phytoplankton species, and are higher in iron-replete than in iron-limited conditions (Strzepek et al., 2005), and carbon:Chl-a (C:Chl-a) ratios increase as Chl-a concentrations decrease (Hewes et al., 1990).

To estimate h for our analysis, we looked at both *in situ* and climatological data. Fig. 5 shows monthly mean estimates of Ona Basin mixed-layer depth for the months of November–April, based on a global climatology by de Boyer Montégut et al. (2004) and a Southern Ocean climatology by Dong et al. (2008). In addition, estimates based on CTD data sampled during the summer 2004 cruise are shown for the months of February and March. Both climatologies use two property-difference criteria for determining mixed-layer depth, one based on density and one on temperature. The density-based criterion defined the base of the mixed layer as the depth at which the potential density increased by 0.03 kg m^{-3} relative to the value at 10 m. The estimates for temperature criterion (not shown) were based on the depth where the absolute change in potential temperature was 0.2 °C, and produced values comparable to the density-based depths. We used the same criteria to compute the summer 2004 estimates.

Using Fe:C ratios ranging from 8 to 22 μmol mol^{-1} and corresponding C:Chl-a ratios ranging from 95 to 72 g^{-1} (Sunda and Huntsman, 2011), and using the Chl-a concentrations in Fig. 3 and the mixed layer depths in Fig. 5, the estimated daily dissolved iron demand in summer ranges from 119 to 247 nmol Fe m^{-2} day^{-1}. This estimate is roughly consistent with Ardelan et al.'s (2010) estimate of approximately 286 nmol Fe m^{-2} day^{-1} in the Bransfield Strait, which is based on new primary production in the region, and Blain et al.'s (2007) estimate of 208 ± 77 nmol Fe m^{-2} day^{-1} in the Kerguelen Plateau, based on the difference between total uptake and regeneration rates of iron. However, the 4-day residence time used in our estimate is based only on the horizontal advection of iron through the region and does not account for remineralization, which may increase the residence time and lower the daily demand estimate.

In order to estimate whether the summertime iron fluxes driven by diapycnal mixing and entrainment can fulfill our estimated demand, we considered the iron concentrations and gradients below the mixed layer in our study region. Fig. 2 shows the location of the iron stations sampled in the Ona Basin during the summer 2004 and winter 2006. The individual profiles for iron stations along a south-to-north transect sampled during the summer 2004 cruise (as shown in Fig. 2A) are plotted in Fig. 6A, and profiles for a transect sampled during the winter 2006 cruise (Fig. 2B) are shown in Fig. 6B. Summer data indicate the presence

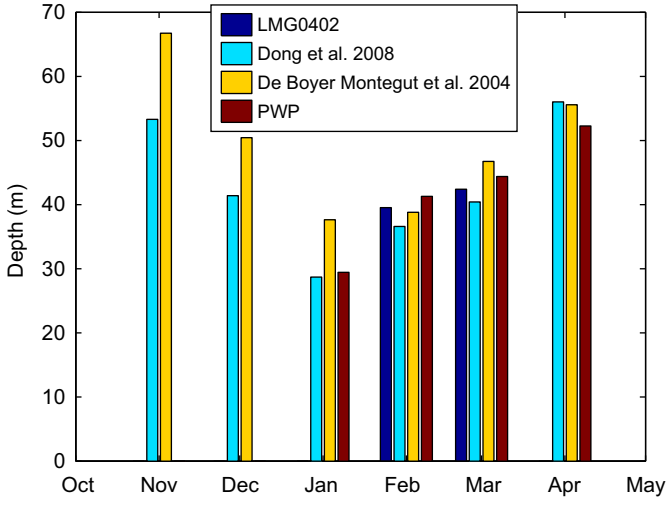

Fig. 5. Density-based monthly mixed-layer depths in the Ona Basin, based on the Dong et al. (2008) Southern Ocean climatology, the de Boyer Montégut et al. (2004) global climatology, the CTD data collected during the summer 2004 cruise, and the output of the Price et al. (1986) (PWP) one-dimensional mixed-layer model.

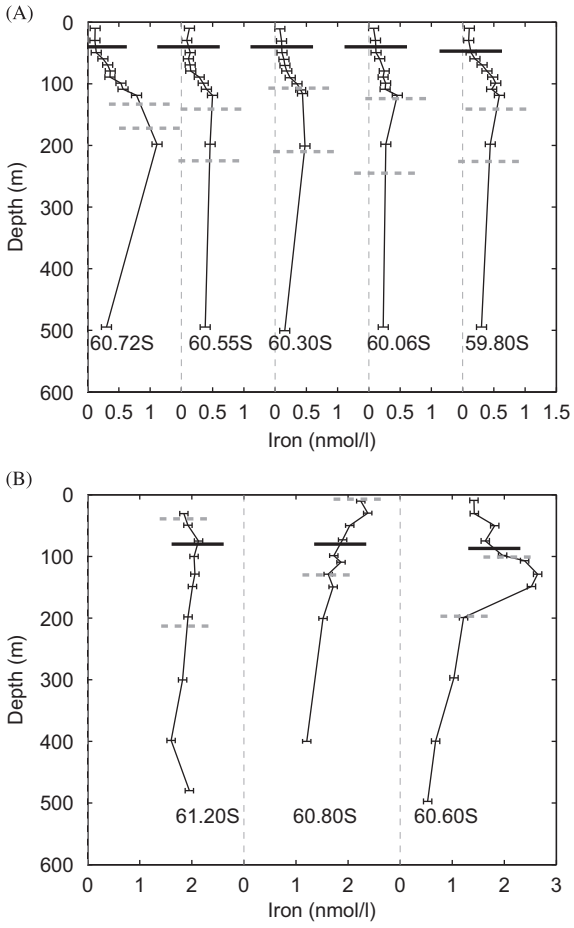

Fig. 6. Cross-shelf transects of dissolved iron profiles in the Ona Basin for (A) summer 2004 and (B) winter 2006. The transects are indicated in red in Fig. 2b. Thick solid horizontal lines indicate density-based mixed layer depth as determined from CTD data at each station, and thick dashed horizontal lines indicate the maximum and minimum depth of the $27.5 \le \sigma_\theta \le 27.6$ density layer. Dashed vertical lines to the left of each profile represent the zero line. Error bars indicate sampling uncertainty as determined by calibration against standard established by the Sampling and Analysis of Iron (SAFe) intercomparison cruise (Johnson et al., 2007).

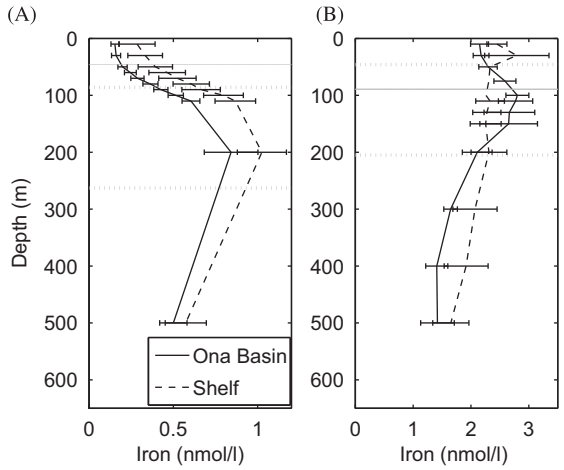

Fig. 7. Mean iron profiles in the Ona Basin and on the continental shelf for (A) summer 2004 and (B) winter 2006. Gray horizontal lines indicate typical mixed layer depth as determined by Dong et al. (2008). The error bars represent the standard error about the mean. Dotted lines indicate the maximum and minimum depth of the $27.5 \leq \sigma_\theta \leq 27.6$ isopycnal.

of high vertical iron gradients in the top 100 m, which can also be seen in the mean profiles computed by averaging all the Ona Basin stations, as shown in Fig. 7A. The highest iron concentrations for the majority of stations sampled both in summer and in winter are found along the $27.5 \leq \sigma_\theta \leq 27.6$ density layer. Ardelan et al. (2010) found high iron concentrations in the same density layer in shelf waters during the austral summer 2006 U.S. Antarctic Marine Living Resources (AMLR) survey. The winter dissolved iron concentrations in the top 200 m are similar in magnitude to the highest summer concentrations, suggesting that the summer peak in the dissolved iron concentration represents the remnant of winter stock.

On average, dissolved iron concentrations are more uniform throughout the water column during winter 2006 than during summer 2004, due to the low summer surface concentrations (Fig. 7). The mean winter iron maximum deepens from a minimum of 30 m on the shelf to 129 m in the Ona Basin, reflecting the increasing depth of the $27.5 \leq \sigma_\theta \leq 27.6$ isopycnal between the station at 60.80°S and 60.60°S, as seen in Fig. 6b. By contrast, the isopycnal depth during the summer 2004 cruise remains roughly the same over the length of the transect shown in Fig. 6A, and the averaged profiles for summer 2004 show the same iron maximum depth for the shelf and Ona Basin stations (Fig. 7A). The northernmost winter station (located at 60.60°S in Fig. 6B) shows a pronounced iron maximum near 150 m, but the surface iron concentration is still similar to the shelf stations, and higher than the summer 2004 surface concentrations shown in Fig. 6A. The differences between the two cruises can be explained by biological uptake of surface iron during the summer. In addition, the $27.5 \leq \sigma_\theta \leq 27.6$ isopycnal is shallower during winter 2006, allowing for isolated storm events as well as diurnal variations in mixed-layer depth to mix more iron toward the surface.

The presence of the summer dissolved iron gradients allows for high upward diffusive fluxes of iron toward the base of the mixed layer and differentiates the Ona Basin from other high-iron regions in the Southern Ocean, such as the Kerguelen Plateau (Blain et al., 2007) and Crozet Plateau (Planquette et al., 2007), where the iron maxima are deeper and iron concentrations in the top 200 m are more uniform, leading to lower estimates of vertical iron fluxes.

Circulation in the basin is characterized by mesoscale eddies that span large depth ranges and can trap water for extended periods of time (Barré et al., 2008; Brandon et al., 2004). Argo float data studied by Barré et al. (2008) showed that floats released in the Ona Basin in March 2002 and December 2003 remained in the basin for periods of 6 months to two and a half years. These numbers suggest that iron entrained near the shelf and advected into the Ona Basin during the winter months can be retained in the basin until the summer, allowing the peaks in the dissolved iron profiles seen in Fig. 6A to persist.

The density distribution and the iron profiles in both summer and winter are consistent with iron being entrained on the shelf and transported along an isopycnal into the Ona Basin. The median depth of the isopycnal during the summer bloom is below the summer mixed layer in the basin. Therefore, some form of vertical mixing is needed to supply the iron into the mixed layer.

One possible mechanism for such vertical mixing is diffusive diapycnal mixing, which has been shown to be elevated over regions of rough bathymetry throughout the Southern Ocean (Sloyan, 2005). Fine-scale estimates of diapycnal diffusivity κ from LADCP and XCTD profiles in Drake Passage indicate the presence of enhanced mixing, with values of κ that have been estimated within the range from $O(10^{-4})$ to $O(10^{-3})$ $m^2\ s^{-1}$ (Naveira Garabato et al., 2004; Thompson et al., 2007). More refined microstructure estimates in Drake Passage yield values of κ on the order of 1×10^{-4} $m^2\ s^{-1}$, reaching 1.3×10^{-4} $m^2\ s^{-1}$ over a transect where the flow regime is similar to our study region, with the ACC flowing over rough topography near the SACCF-n. (St. Laurent, submitted for publication). Given these diffusivity estimates and the mean Ona Basin iron profiles in Fig. 7, and assuming no horizontal advection, the vertical diffusive flux F_z of dissolved iron can be computed as

$$F_z = -\kappa \frac{\partial Fe}{\partial z}. \tag{2}$$

Assuming a diffusivity at the lower end of the estimated range ($\kappa = 1 \times 10^{-4}$ $m^2\ s^{-1}$) and solving Eq. (2) for the averaged dissolved iron profiles shown in Fig. 7 with the vertical iron gradient computed between 50 and 100 m, where the iron profiles are monotonic, gives an estimated iron flux of 64 ± 2 nmol $m^{-2}\ day^{-1}$ into the base of the summer mixed layer.

Changes in mixed-layer depth provide an additional mechanism for increasing dissolved iron concentrations near the surface. As the mixed layer deepens, it entrains iron from the top of the pycnocline and mixes it toward the surface. This additional entrainment can help compensate for decreasing iron concentrations and reduced near-surface gradients as iron is consumed over the summer.

In November and December, when correlations between SACCF-n position and Chl-a concentration are highest, the mixed layer depths shown in Fig. 5 grow shallower, indicating that entrainment is unlikely to supply iron to the euphotic zone. Starting in January and continuing until the end of the summer, the mixed layer deepens as the correlations between frontal position and Chl-a decrease, and the high Chl-a levels persist. This pattern is consistent with a scenario in which mixed-layer entrainment provides the additional iron needed to sustain the bloom in the Ona Basin during the months when horizontal advection no longer explains the persistence of the bloom.

Given the monthly mixed-layer depth changes seen in Fig. 5 and the mean iron profiles in Fig. 7, it is possible to estimate a mean daily entrainment rate for iron into the base of the mixed layer. The mean concentration of iron in the mixed layer can be calculated as

$$\mathrm{Fe}_{ml} = \frac{\int_0^h \mathrm{Fe}\, dz}{h}, \tag{3}$$

where h is the mixed-layer depth.

The mean daily entrainment rate E over a period of n days can then be calculated as

$$E = \frac{Fe_{ml}(n) - Fe_{ml}(0)}{n}, \quad (4)$$

where $Fe_{ml}(i)$ is the mixed-layer iron concentration on the ith day.

If we assume that the mixed-layer changes steadily and monotonically over the course of each month, then applying Eq. (4) to the climatological and *in situ* depths shown in Fig. 5 and the averaged mixed-layer dissolved iron concentrations computed from the profiles in Fig. 6A yields daily entrainment rates ranging from 5 to 25 nmol m^{-2} day^{-1}. However, such an assumption does not reflect the diurnal mixed-layer cycle or the impact of isolated storm events that may cause large changes in the mixed-layer depth over a short period of time. In the next section, we use a one-dimensional numerical model to take these additional variables into account.

3.3. Results from one-dimensional model simulation

If diffusivity in our study region is assumed to be close to St. Laurent's (submitted for publication) observed values of 1×10^{-4} m^2 s^{-1}, neither diapycnal mixing nor mixed-layer entrainment alone would appear to be sufficient to sustain the Ona Basin Chl-a levels during the late summer months. However, these two processes can combine non-linearly, especially if short-term variations in mixed-layer depth are taken into account. Isolated weather events can lead to short-term deepening of the mixed layer, entraining additional iron. The effects of such events cannot be estimated from monthly averages. To evaluate these effects, we performed a numerical simulation using a modified version of the one-dimensional mixed-layer model developed by Price et al. (1986, henceforth PWP).

The PWP model was originally intended to compute the diurnal variability of the mixed-layer depths. It accepts a time series of forcing variables consisting of winds, precipitation and surface heat fluxes, and applies them to mix initial profiles of temperature and salinity. For our analysis, we modified the model to accept an additional input of an initial iron profile, created from the averaged profile shown in Fig. 7A by using a linear fit to interpolate the data to 5 m resolution. The initial temperature and salinity profiles, made by averaging all available summer 2004 profiles in the Ona Basin and also interpolated to 5 m resolution, are shown in Fig. 8. Our simulation was run for 120 days, with a time step of 10 min and a depth increment of 5 m, to a maximum depth of 500 m, as most of the iron profiles were not sampled below that depth.

To account for diapycnal mixing, we modified PWP to incorporate the vertical diffusive flux of iron as defined in Eq. (2) and to solve for F_z at each time step. We then ran the model for two configurations: one without the flux modification ($\kappa = 0$), to yield an estimate of mixed-layer iron concentrations based only on entrainment; and one using the modified model with vertical diffusion to provide an estimate of diapycnal mixing and entrainment combined. Five values of κ were tested, ranging from 5×10^{-5} m^2 s^{-1} to 2×10^{-4} m^2 s^{-1}, in order to consider a range of values that extended beyond the 1×10^{-4} m^2 s^{-1} estimate reported by St. Laurent (submitted for publication).

For our simulations we set boundary conditions $\partial Fe/\partial z = 0$ and $\partial^2 Fe/\partial z^2 = 0$ to ensure no diffusive flux at the bottom of the water column or through the base of the mixed layer. The results were not strongly sensitive to this boundary condition choice: eliminating the $\partial^2 Fe/\partial z^2 = 0$ requirement or shifting the top-most boundary condition for our simulation from the base of the mixed layer to the ocean surface resulted in differences of less than 10 nmol m^{-2} day^{-1} in the entrainment rates.

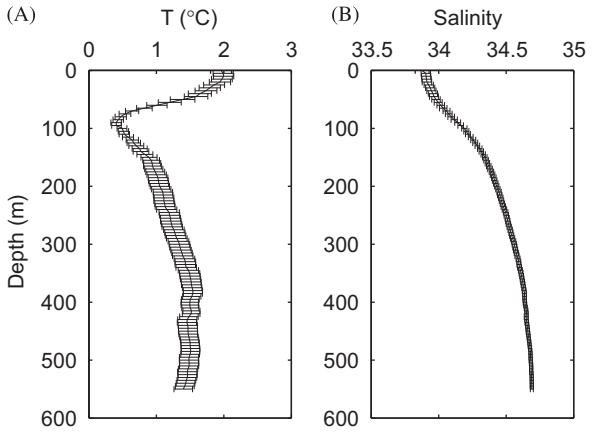

Fig. 8. (A) Temperature and (B) salinity profiles used as inputs for the PWP model. The error bars represent the standard error about the mean.

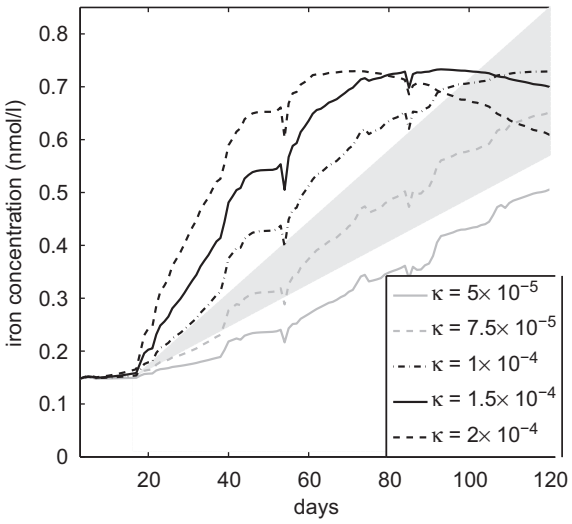

Fig. 9. Daily mixed-layer iron concentrations computed by the modified Price et al. (1986) (PWP) one-dimensional mixed-layer model for five values of diapycnal diffusivity κ, using a combination of diapycnal mixing and mixed-layer entrainment. The shaded gray area beginning at day 16 represents the range of iron demand rates derived from Eq. (1).

To determine the uncertainties for our results, we performed a Monte Carlo simulation in which the PWP model was run 100 times for each of the scenarios described above. For each the original iron input was perturbed by a vector of normally distributed random numbers scaled to match the mean standard deviation of the iron profiles shown in Fig. 7A. We then computed the mean daily entrainment of iron for each run, and used the standard deviation of the result as the uncertainty for our original estimate.

The entrainment-only PWP simulation produced a mean daily entrainment rate of 12 ± 9 nmol m^{-2} day^{-1}, consistent with the rates derived from the mixed layer estimates in Section 3.2.

For the diffusive version of the PWP-model, time-series of mixed-layer iron "concentrations" are shown in Fig. 9 for five values of κ, here plotted for the limiting case where there is no biological consumption. The slopes of the lines in Fig. 9 provide a measure of the iron-supply rate, while the gray region delineates the range of iron demand rates derived from Eq. (1). (If biological uptake of iron were included, iron concentrations would not increase continuously but would be expected to be near zero all of the time.) For all values of κ, the mixed-layer iron concentration begins to rise approximately 16 days into the 120-day model run. For lower values of κ, the concentration steadily increases throughout the run. The smallest

non-zero κ ($\kappa = 5 \times 10^{-5}$ m^2 s^{-1}) yields a time-averaged iron supply rate of 106 ± 22 nmol m^{-2} day^{-1}, insufficient to meet the iron demand estimated from Eq. (1). In contrast, for $\kappa = 1 \times 10^{-4}$ m^2 s^{-1}, the mean daily iron supply rate is 180 ± 46 nmol m^{-2} day^{-1}, which is well within the iron demand range from Eq. (1). The averaged monthly mixed-layer depths produced by the diffusive PWP model for $\kappa = 1 \times 10^{-4}$ m^2 s^{-1} are shown in Fig. 5. The mixed-layer depths are comparable to the climatology-derived depths, as well as observed depths from the summer 2004 cruise.

For larger values of κ, mixed-layer iron concentrations in the PWP simulations initially rise, and then once diffusion has eroded the subsurface iron maxima, the iron concentrations decrease. For example, for $\kappa = 2 \times 10^{-4}$ m^2 s^{-1}, the iron supply rate is 293 ± 44 nmol m^{-2} day^{-1}, exceeding the highest of our iron demand estimates, for the first 73 days of the 120-day PWP run, before the iron concentration begins to decrease. Such a time scale is too short to allow continued input of iron to the mixed-layer for the duration for the extended summer bloom seen in southern Drake Passage. The largest diffusivity that produces steadily increasing mixed-layer iron concentrations for at least 90 days is $\kappa = 1.5 \times 10^{-4}$ m^2 s^{-1}. This value of κ will exceed the estimated iron demand for the first 85 days of the model run, producing a mean daily iron supply rate of 250 ± 28 nmol m^{-2} day^{-1}. Over 90 days, representing the period from January until the end of March, this value produces a mean supply rate of 230 ± 23 nmol m^{-2} day^{-1}, close to the maximum of the iron demand range from Eq. (1).

These results indicate that a diffusivity from $\kappa = 7.5 \times 10^{-5}$ to 1.5×10^{-4} m^2 s^{-1} will meet or exceed the Ona Basin bloom throughout the summer via diapycnal mixing and entrainment. Smaller values of κ yield too little iron, and larger values erode the subsurface iron maximum too quickly. This range is roughly consistent with the diffusivities inferred from microstructure measurements in the Drake Passage region (St. Laurent, submitted for publication). These results are derived assuming that the along-isopycnal iron advection does not play a significant role in sustaining the bloom to the end of summer. If along-isopycnal advection were significant that could resupply the subsurface iron maximum and reduce the possibility that high diffusivities might too quickly erode the subsurface iron maximum.

3.4. Discussion

The mixing and entrainment processes discussed in the preceding sections are purely physical, and do not take into account the impact of biogeochemical processes on mixed-layer iron supply or the effects of possible changes in the phytoplankton community on iron demand as the bloom progresses. However, the results of our numerical simulation indicate that physical processes alone can potentially deliver iron into the mixed layer at a rate that meets or exceeds the estimated iron demand during the summer. Therefore, during periods when the diffusivity in the Ona Basin is within the range of typically observed values, the physical processes in the basin appear sufficient to sustain the summer bloom for as long as the near-surface iron gradients persist. This does not exclude the possibility that biogeochemical processes, which are always present alongside the physical processes, may also play an important role in controlling iron supply in the Ona Basin euphotic zone. In particular, when the demand is closer to the high estimate or the diffusivity is either too high to sustain the vertical iron gradients or too low to provide a sufficiently large iron flux into the mixed layer, additional contributions from biogeochemical processes such as grazing and remineralization may be necessary. Particulate iron, not sampled in this study, could also be delivered into the mixed layer by the same physical processes that we describe in our analysis, and provide an additional source to bring the iron supply closer to the upper range of our estimated demand.

4. Summary

Satellite-derived Chl-a concentrations from November to April are consistently higher in the waters to the east of the Shackleton Transverse Ridge than in the waters to the west. The northern branch of the Southern ACC Front, as defined by the 64-cm sea-surface height contour, moves off-shore east of the ridge. Because this branch functions as the barrier between the ACC and the iron-rich shelf water to the south, the fraction of the Ona Basin where sea-surface height is less than 64 cm can be used as an estimate of the fraction of shelf water in the surface waters of the basin. Comparison between sea-surface height and Chl-a data shows that the fraction of shelf waters present in the Ona Basin is highly correlated with Chl-a concentration during the months of November and December. The correlations become smaller from January onward, while Chl-a levels in the Ona Basin rise slightly, and the ratio of mean Chl-a east of the ridge to mean Chl-a west of the ridge increases. These results are consistent with a scenario in which horizontal advection of shelf waters can account for the intensity of the spring bloom in the Ona Basin, but this advection alone is not sufficient to sustain the bloom through the end of the summer.

Iron profiles in the Ona Basin during both winter 2006 and summer 2004 show a strong subsurface maximum between 100 and 200 m, and high near-surface gradients that persist from winter into summer, allowing a vertical flux of iron to the base of the mixed layer due to diapycnal mixing. The mixed layer in the Ona Basin also deepens from January into April, after becoming shallower from November to January. The increased mixed-layer depth provides an additional mechanism to supply iron to the surface, by allowing it to be entrained from the top of the pycnocline. Estimates of the mean daily entrainment rate and the diffusive iron flux with diapycnal diffusivity $\kappa = 1.0 \times 10^{-4}$ m^2 s^{-1} indicate that neither process alone appears sufficient to sustain the summer bloom in the Ona Basin. However, a numerical simulation suggests that entrainment in combination with values of κ between 7.5×10^{-5} and 1.5×10^{-4} m^2 s^{-1} can supply enough iron into the top 30 m of the basin to meet or exceed the iron demand of the bloom. These diffusivities are typical of diffusivity estimates derived from microstructure measurements in the Drake Passage region. A number of other mechanisms, including biogeochemical processes, atmospheric dust deposition, and additional vertical mixing associated with mesoscale eddies, could further contribute to iron availability in the region, and would be necessary to sustain the bloom during times when the iron demand is high or the diffusivity in the region falls outside our estimated range.

Acknowledgments

The authors would like to thank the crews of the R/V Laurence M. Gould and R/V Nathaniel B. Palmer, the employees of the Raytheon Polar Services Company, and Katherine Barbeau of Scripps Institution of Oceanography. NCEP Reanalysis data were provided by the NOAA/OAR/ESRL PSD, Boulder, Colorado, USA, from their Web site at http://www.esrl.noaa.gov/psd/. This research was supported by the US National Science Foundation (grants OPP-0230443, ANT-0444134, ANT-0948338, OCE-0622740 and OCE-0957342).

References

Abraham, E.R., Law, C.S., Boyd, P.W., Lavender, S.J., Maldonado, M.T., Bowie, A.R., 2000. Importance of stirring in the development of an iron-fertilized phytoplankton bloom. Nature 407, 727–729.

Ardelan, M.V., Holm-Hansen, O., Hewes, C.D., Reiss, C.S., Silva, N.S., Dulaiova, H., Steinnes, E., Sakshaug, E., 2010. Natural iron enrichment around the Antarctic Peninsula in the Southern Ocean. Biogeosciences 7, 11–25.

Barbeau, K., Kujawinski, E.B., Moffett, J.W., 2001. Remineralization and recycling of iron, thorium and organic carbon by heterotrophic marine protists in culture. Aquat. Macrob. Ecol. 24, 69–81.

Barré, N., Provost, C., Sennechael, N., Lee, J.H., 2008. Circulation in the Ona Basin, southern Drake Passage. J. Geophys. Res. 113, c04033, http://dx.doi.org/10.1029/2007JC004549.

Blain, S., Queguiner, B., Armand, L., Belviso, S., Bombled, B., Bopp, L., Bowie, A., Brunet, C., Brussaard, C., Carlotti, F., Christaki, U., Corbiere, A., Durand, I., 2007. Effect of natural iron fertilization on carbon sequestration in the Southern Ocean. Nature 446, 1070–1074.

Blain, S., Sarthou, G., Laan, P., 2008. Distribution of dissolved iron during the natural iron-fertilization experiment KEOPS (Kerguelen Plateau, Southern Ocean). Deep-Sea Res. II 55, 594–605.

Bowie, A.R., Maldonado, M.T., Frew, R.D., Croot, P.L., Achterberg, E.P., Mantonura, R.F.C., Worsfold, P.J., Law, C.S., Boyd, P.W., 2001. The fate of added iron during a mesoscale fertilisation experiment in the Southern Ocean. Dee-Sea Res. II 48, 2703–2743.

Boyd, P.W., 2002. The role of iron in the biogeochemistry of the Southern Ocean and equatorial Pacific: a comparison of in situ iron enrichments. Deep-Sea Res. II, 1803–1821.

Brandon, M.A., Naganobu, M., Demer, D.A., Chernyshkov, P., Trathan, P.N., Thorpe, S.E., Kameda, T., Berezhinskiy, O.A., Hawker, E., Grant, S., 2004. Physical oceanography in the Scotia Sea during the CCAMLR 2000 survey, austral summer 2000. Deep-Sea Res. II 51, 1301–1321.

Chisholm, S.W., Morel, F.M.M., 1991. What controls phytoplankton production in nutrient-rich areas of the open sea? Limnol. Oceanogr. 36, 1507–1511.

Dalbec, A.A., Twining, B.S., 2009. Remineralization of bioavailable iron by a heterotropic dinoflagellate. Aquat. Microb. Ecol. 54, 279–290.

de Baar, H.J.W., de Jong, J.T.M., Bakker, D.C.E., Loscher, B.M., Veth, C., Bathmann, U., Smetacek, V., 1995. Importance of iron for plankton blooms and carbon dioxide drawdown in the Southern Ocean. Nature 373, 412–415.

de Boyer Montégut, C., Madec, G., Fischer, A.S., Lazar, A., Iudicone, D., 2004. Mixed layer depth over the global ocean: an examination of profile data and a profile-based climatology. J. Geophys. Res. 109, 55, http://dx.doi.org/10.1029/2004JC002378.

Dong, S., Sprintall, J., Gille, S.T., Talley, L., 2008. Southern Ocean mixed-layer depth from Argo float profiles. J. Geophys. Res. 113, c06013, http://dx.doi.org/10.1029/2006JC004051.

Ducet, N., LeTraon, P.-Y., Reverdin, G., 2000. Global high resolution mapping of ocean circulation from Topex/Poseidon and ERS-1 and -2. J. Geophys. Res. 105, 19477–19498.

Dulaiova, H., Ardelan, M.V., Henderson, P.B., Charette, M.A., 2009. Shelf-derived iron inputs drive biological productivity in the southern Drake Passage. Glob. Biogeochem. Cycles 23, gB4014, http://dx.doi.org/10.1029/2008GB003406.

Frants, M., Gille, S.T., Hewes, C.D., Holm-Hansen, O., Kahru, M., Lombrozo, A., Measures, C.I., Mitchell, G.B., Wang, H., Zhou, M., 2013. Optimal Multiparameter analysis of source water distributions in the southern Drake Passage. Deep-Sea Res. II 90, 31–42.

Gasso, S., Stein, A.F., 2007. Does dust from Patagonia reach the sub-Antarctic Atlantic Ocean? Geophys. Res. Lett. 34, l01801, http://dx.doi.org/10.1029/2006GL027693.

Gouretski, V.V., Koltermann, K.P., 2004. WOCE Global Hydrographic Climatology. Technical Report 35/2004, Berichte des Bundesamtes fur Seeschifffahrt und Hydrographie, Hamburg, Germany.

Helbling, E.W., Villafane, V., Reid, F.M.H., Holm-Hansen, O., 1991. Effect of iron on productivity and size distribution of Antarctic phytoplankton. Limnol. Oceanogr. 36, 1879–1885.

Hewes, C.D., Saksahaug, E., Reid, F.M.H., Holm-Hansen, O., 1990. Microbial autotrophic and heterotrophic eucaryotes in Antarctic waters: relationships between biomass and chlorophyll, adenosine triphosphate and particulate organic carbon. Mar. Ecol. Prog. Ser. 63, 27–35, http://dx.doi.org/10.3354/meps063027.

Holm-Hansen, O., Kahru, M., Hewes, C.D., 2005. Deep chlorophyll a maxima ccDCMSscc in pelagic Antarctic waters. II. Relation to bathymetric features and dissolved iron concentrations. Mar. Ecol. Prog. Ser. 297, 71–81.

Holm-Hansen, O., Kahru, M., Hewes, C.D., Kawaguchi, S., Kameda, T., Sushin, V., Krasovski, I., Priddle, J., Korb, R., Hewitt, R.P., Mitchell, B.G., 2004a. Temporal and spatial distribution of chlorophyll-a in surface waters of the Scotia Sea as determined by both shipboard measurements and satellite data. Deep-Sea Res. II 51, 1323–1331.

Holm-Hansen, O., Naganobu, M., Kawaguchi, S., Kameda, T., Krasovski, I., Tchernyshkov, P., Priddle, J., Korb, R., Brandon, M., Demer, D., Hewitt, R.P., Kahru, M., Hewes, C.D., 2004b. Factors influencing the distribution, biomass, and productivity of phytoplankton in the Scotia Sea and adjoining waters. Deep-Sea Res. II 51, 1333–1350.

Hopkinson, B.M., Mitchell, G.B., Reynolds, R.A., Wang, H., Measures, C.I., Selph, K.E., Hewes, C.D., Holm-Hansen, O., Barbeau, K.A., 2007. Iron limitation across chlorophyll gradients in the southern Drake Passage: Phytoplankton responses to iron addition and photosynthetic indicators of iron stress. Limnol. Oceanogr. 52, 2540–2554.

Hughes, C.W., Ash, E., 2001. Eddy forcing of the mean flow in the Southern Ocean. J. Geophys. Res. 106, 2713–2722.

Johnson, K.S., Boyle, E., Bruland, K., Coale, K., Measures, C., Moffett, J., Aguilar-Islas, A., Barbeau, K., Bergquist, B., Bowie, A., Buck, K., Cai, Y., Chase, Z., Cullen, J., Doi, T., Elrod, V., Fitzwater, S., Gordeon, M., King, A., Laan, P., Laglera-Baquer, L., Landing, W., Lohan, M., Mendez, J., Milne, A., Obata, H., Ossiander, L., Plant, J., Sarthou, G., Sedwick, P., Smith, G.J., Sohst, B., Tanner, S., Van den Berg, S., Wu, J., 2007. Developing standards for dissolved iron in seawater. EOS 88 (11), 131–132.

Kahru, M., Mitchell, B.G., 2006. Satellite observations of fronts in the Drake Passage: Implications for carbon cycling. In: EOS Transaction AGU 87(36), Ocean Sciences Meeting Supplement, AGU, Abstract OS54D-01.

Kahru, M., Mitchell, B.G., Gille, S.T., Hewes, C.D., Holm-Hansen, O., 2007. Eddies enhance biological production in the Weddell-Scotia Confluence of the Southern Ocean. Geophys. Res. Lett. 34, l14603, http://dx.doi.org/10.1029/2007GL030430.

Kalnay, E., coauthors, 1996. The NCEP/NCAR 40-year reanalysis project. Bull. Am. Meteorol. Soc. 77, 437–471.

Lapeyre, G., Klein, P., 2006. Impact of the small-scale elongated filaments on the oceanic vertical pump. J. Mar. Res. 64, 835–851.

Maraldi, C., Mongin, M., Coleman, R., Testut, L., 2009. The influence of lateral mixing on a phytoplankton bloom: distribution in the Kerguelen Plateau region. Deep-Sea Res. I 56, 963–973.

Martin, J., Gordon, R., Fitzwater, S., 1990. Iron in Antarctic waters. Nature 345, 156–158.

Measures, C.I., Brown, M.T., Selph, K.E., April, A., Zhou, M., Hatta, M., Hiscock, W.T., 2013. The influence of shelf processes in delivering dissolved iron to the HNLC waters of the Drake Passage Antarctica. Deep-Sea Res. II 90, 77–88.

Measures, C.I., Landing, W.M., Brown, B.C., 2008. A commercially available rosette system for trace metal clean sampling. Limnol. Oceanogr. Methods 6, 384–394.

Mongin, M., Molina, E., Trull, T.W., 2008. Seasonality and scale of the Kerguelen Plateau phytoplankton bloom: a remote sensing and modeling analysis of the influence of natural iron fertilization in the Southern Ocean. Deep-Sea Res. II 55, 880–892.

Naveira Garabato, A.C., Polzin, K.L., King, B.A., Heywood, K.J., Visbeck, M., 2004. Widespread intense turbulent mixing in the Southern Ocean. Science 303, 210–213.

O'Reilly, J.E., Maritorena, S., Mitchell, B.G., Siegel, D.A., Carder, K.L., Garver, S.A., Kahru, M., McClain, C., 1998. Ocean color chlorophyll algorithms for SeaWiFS. J. Geophys. Res. 103, 24,937–24,953.

Orsi, A.H., Whitworth, T., Nowlin, W.D., 1995. On the meridional extent and fronts of the Antactic Circumpolar Current. Deep-Sea Res. I 42, 641–673.

Planquette, H., Statham, P.J., Fones, G.R., Charette, M.A., Moore, C.M., Salter, I., Nedelec, F.H., Taylor, S.L., French, M., Baker, A.R., Mahowald, N., Jickells, T.D., 2007. Dissolved iron in the vicinity of the Crozet Islands, Southern Ocean. Deep-Sea Res. II 54, 1999–2019.

Price, J.F., Weller, R.A., Pinkel, R., 1986. Diurnal cycling: Observation and models of the upper ocean response to diurnal heating, cooling and wind mixing. J. Geophys. Res. 91, 8411–8427.

Sloyan, B., 2005. Spatial variability of mixing in the Southern Ocean. Geophys. Res. Lett. 32 10.10292005GL023568.

Sokolov, S., Rintoul, S.R., 2007. Multiple jets of the Antarctic circumpolar current south of Australia. J. Phys. Oceanogr. 37, 1394–1412.

Sokolov, S., Rintoul, S.R., 2009. Circumpolar structure and distribution of the Antarctic circumpolar current fronts: 2. Variability and relationship to sea surface height. J. Geophys. Res. 114, c1109, http://dx.doi.org/10.1029/2008JC005428.

St. Laurent, L.C., Naveira Garabato, A.C., Ledwell, J.R., Thurnherr, A.M., Toole, J.M. Turbulence and diapycnal mixing in Drake Passage. J. Phys. Oceanogr., submitted for publication.

Strzepek, R.F., Maldonado, M.T., Higgins, J.L., Hall, J., Safi, K., Wilhelm, S.W., Boyd, P.W., 2005. Spinning the 'Ferrous Wheel': the importance of the microbial community in an iron budget during the FeCycle experiment. Glob. Biogeochem. Cycles 19, GB4S26, http://dx.doi.org/10.1029/2005GB002490.

Sunda, W.G., Huntsman, S.A., 2011. Interactive effects of light and temperature on iron limitation in a marine diatom: Implications for marine productivity and carbon cycling. Limnol. Oceanogr. 56, 1475–1488.

Thompson, A.F., Gille, S.T., MacKinnon, J.A., Sprintall, J., 2007. Spatial and temporal patterns of small-scale mixing in Drake Passage. J. Phys. Oceanogr. 37, 572–592.

Venables, H.J., Pollard, R.T., Popova, E.E., 2007. Physical conditions controlling the development of a regular phytoplankton bloom north of the Crozet Plateau, Southern Ocean. Deep-Sea Res. II 54, 1949–1965.

Whitehouse, M.J., Korb, R.E., Atkinson, A., Thorpe, S.E., Gordon, M., 2008. Formation, transport and decay of an intense phytoplankton bloom within the high-nutrient low-chlorophyll belt of the Southern Ocean. J. Mar. Syst. 70, 150–167.

Yelland, M., Moat, B.I., Taylor, P.K., Pascal, R.W., Hutchings, J., Cornell, V.C., 1998. Wind stress measurements from the open ocean corrected for airflow distortion. J. Phys. Oceanogr. 28, 1511–1526.

Yelland, M., Taylor, P.K., 1996. Wind stress measurements from the open ocean. J. Phys. Oceanogr. 26, 541–558.

Zhou, M., Zhu, Y., Dorland, R., 2010a. Dynamics of the current system in the Southern Drake Passage. Deep-Sea Res. 57, 1039–1048.

Zhou, M., Zhu, Y., Dorland, R.D., Measures, C.I., 2010b. Dynamics of the current system in the southern Drake Passage. Deep-Sea Res. I 57, 1039–1048.